J Solid State Electrochem (2000) 4: 306–313

ORIGINAL PAPER

Snejana Bakardjieva · Petr Bezdička · Tomáš Grygar
Petr Vorm

Reductive dissolution of microparticulate manganese oxides

Received: 11 October 1999 / Accepted: 2 December 1999

Abstract Electrochemical dissolution of immobilised microparticulate Mn(III,IV) oxides in slightly acidic solution (pH 4.4) was found to be a very general reaction, which is responsible for well-defined voltammetric peaks. Dissolution of six Mn(III,IV) oxides is initiated by the reduction of Mn(IV) to Mn(III) in the solid phase, which is followed by a massive dissolution via further reduction of Mn(III) to Mn(II), which finally yields soluble Mn^{2+}. The reactivity of manganese oxides depends on their structure: the most reactive are amorphous (δ-MnO_2) and layered structures (birnessite); more resistant toward reductive dissolution are α- and λ-MnO_2 and electrochemical manganese dioxide; and least reactive is β-MnO_2. Reductive dissolution of $LiMn_2O_4$ resembles that of λ-MnO_2, whereas $CaMnO_3$ dissolves via a different reaction mechanism.

Key words Manganese oxides · Reductive dissolution

Introduction

Mn(II,III,IV) oxides occur in numerous phases of extremely variable structures [1–3], that are enabled by the ability of their building unit, $Mn(O,OH)_6$ octahedra, to form infinite layers and three-dimensional structures. These structures usually contain relatively freely accessible tunnels and/or interlayer spaces of various sizes, that both can serve as a suitable space for ion insertion. Continuous interest in electrochemical characterisation of manganese oxides is mainly caused by their common application in primary and secondary batteries [4]. The experimental techniques and data evaluation have hence been focused on such properties like cell voltage, depth of discharge and cycle number, and individual Mn oxide phases are commonly evaluated with a particular respect to their practical application. Particularly γ-MnO_2, ramsdellite, so-called electrochemical manganese dioxide (EMD), and β-MnO_2 (pyrolusite) have been studied [5, 6]. Several new findings have recently refreshed the interest in electrochemistry of Mn oxides: the development of secondary cells with EMD [7], proposals to employ Bi-doped birnessite in secondary cells [8] and perovskite $CaMnO_3$ in primary cells [9], and attempts to utilise practically the reversible insertion of Li^+(aq) into spinel-type Mn oxides [3, 10, 11].

The most frequently studied reaction used for comparison of Mn oxide phases is their solid-state redox reaction in alkaline solution [5–8, 10–15], i.e., the reaction proceeding in primary and secondary batteries. The solid-state redox cycling of Mn(II) in neutral supporting electrolyte was recently proposed for rapid characterisation of tunnelled Mn oxides [16]. According to the authors [16], voltammetry could become a very valuable contribution to other techniques of analysis of new synthetic Mn oxides. This is particularly attractive with respect to the similarity of powder X-ray diffraction (XRD) patterns of individual Mn oxides [1] and generally poor crystallinity of the practically used electrode materials.

Cyclic voltammetry with electrodes of MnO_x and C mixtures is the most common experimental technique employed for electrochemical studies of Mn oxides [6–8, 10, 12, 13, 16]. A different, very simple experimental technique, referred to as voltammetry of immobilised microparticles, has been developed by Scholz and coworkers in the past decade [17, 18]. Voltammetry of immobilised microparticles was already proposed for rapid evaluation of battery Mn oxides [14, 15] and for characterisation of naturally occurring Mn phases [19]. The applicability of this versatile technique is wider than that of carbon paste or other composite electrodes, and so the former technique has already been applied to a

Presented at the international conference "Modern Electroanalytical Methods", 19th to 23rd September, 1999, in Seč, Czech Republic

S. Bakardjieva · P. Bezdička · T. Grygar (✉) · P. Vorm
Institute of Inorganic Chemistry,
Czech Academy of Sciences, 250 68 Řež, Czech Republic
e-mail: grygar@iic.cas.cz

very wide range of microparticulate electroactive solids [18]. Voltammetry of microparticles is particularly suitable for the monitoring of the reductive decay of Mn oxides [14, 15, 20], reductive dissolution of Fe(III) oxides [21, 22], and oxidative dissolution of metals [23, 24], sulfides [25], and Cr(III,IV) oxides [26]. Surprisingly, reductive dissolution of Mn(III,IV) oxides has not been systematically evaluated for the purpose of analysis and purification of synthetic samples, although these reactions are commonly used, e.g., for Fe oxides. We hence studied reductive dissolution of several Mn(III,IV) oxides using voltammetry of microparticles. We compared layered oxides of birnessite-type (0.7 nm interlayer distance), three-dimensional Mn oxides with tunnels of various sizes (α-MnO_2, β-MnO_2, and EMD), spinel $LiMn_2O_4$ and perovskite $CaMnO_3$. To be able to directly compare the electrochemical reactivity of the powdered samples of various crystallinity and phase composition, we used a combination of cyclic voltammetry and potential pulse chronoamperometry.

Experimental

Synthetic methods used for sample preparation are summarised in Table 1.

α-MnO_2 (K-forms, cryptomelane)

Cry1 was obtained by a wet synthetic method described in [27] (sample 3). $KMnO_4$ (9 g) in warm water 100 ml was reduced by 6 M HCl (50 ml). The solid intermediate was digested with excess of 3 M HNO_3 at 90 °C for 5 h.

Cry2 was obtained from $KMnO_4$ by a sol-gel process similar to that described [28–30]. The gel precursor was obtained be mixing $KMnO_4$ (3 g) in water 50 ml with glycerol (1 g) in water 20 ml. The resulting gel was heated on a hot plate, decanted and then left to dry. The residue was calcined at 450 °C, then dispersed in distilled water, filtered, washed with water and the product dried at 110 °C.

Cry3 was prepared by evaporation of solution containing $Mn(NO_3)_2$, KNO_3, and citric acid on a hot plate, burning the resulting foam at about 300 °C, and finally calcining the ash at 500 °C.

β-MnO_2 (pyrolusite)

The sample of Pyr was prepared by common thermal decomposition of $Mn(NO_3)_2 \cdot 4H_2O$ ([27], sample 12). The Mn nitrate was melted in its crystal water, then dried on a hot plate; the residue was suspended in distilled water, filtered, washed with water, and then heated at 170 °C.

Electrochemical manganese dioxides

Two commercial samples, EMD1 and EMD2, were supplied by TOSOH Hellas (Greece) and by Lachema (Czech Republic), respectively. The samples were ground in an agate mortar before use.

Birnessite

Bir1 was prepared by oxidation of Mn^{2+} in alkaline medium [31]. 3%H_2O_2 (100 ml) with 0.6 M NaOH was poured into 0.3 M $Mn(NO_3)_2$ (50 ml) under intensive stirring. The suspension was left to cool and the solid was filtered, washed with water and dried at 110 °C.

Bir2 was prepared by a sol-gel procedure based on reduction of $KMnO_4$ [32]. A solution of $KMnO_4$ (3 g) in H_2O (50 ml) was quickly added to 1.4 M glucose (50 ml) under intensive stirring for 10–15 s. The gel was formed within several tens of seconds. The gel was heated on a hot plate, decanted, and then left to dry. The dry intermediate was calcined for 2 h at 400 °C, then ground. Excess K^+ was washed with water and the product was dried at 110 °C.

$LiMn_2O_4$ (Sp) and $CaMnO_3$ (Per1) were prepared similarly as Cry3 by evaporation of corresponding nitrates with citric acid, burning, and then calcining the solid intermediates. The final temperatures of calcination were 850 °C or 400 °C for Li manganite, and 900 °C for Ca-Mn perovskite, respectively. $CaMnO_3$ (samples Per2 and Per3) were prepared by thermal decomposition of co-precipitated carbonates. A sample of λ-MnO_2 (Sp4) was prepared by ion exchange of $LiMn_2O_4$ with diluted HCl [33].

Sample characterisation

Solid phases were identified using powder XRD analysis (Siemens D5005, Germany). Titration analysis and flame emission photometry were used to determine the elemental composition and Mn valence of the oxides. Total Mn was determined by chelatometric titration, Mn valence by iodometric titration, Li, Na, K, and Ca by flame photometry. The particle size was checked using transmission

Table 1 Overview of the samples studied

Sample	Synthesis	Final temperature	Phase identification (XRD)	Formula
EMD1	Commercial sample	–	Nsutite (PDF 17-0510)	$MnO_{2.00}$
EMD2	Commercial sample	–	Nsutite (PDF 17-0510)	$MnO_{1.97}$
Pyr	Heating $Mn(NO_3)_2$	170 °C	Pyrolusite (PDF 24-735)	$MnO_{1.98}$
Bir1	Wet method	110 °C	Turbostratic birnessite [36]	$Na_{0.31}MnO_{2.00}$
Bir2	Sol-gel	400 °C	Hexagonal birnessite [36]	$K_{0.25}MnO_{1.94}$
Cry1	Wet method	110 °C	Cryptomelane (PDF 12-706)	$K_{0.07}MnO_{1.98}$
Cry2	Sol-gel	450 °C	Cryptomelane (PDF 29-1020)	$K_{0.11}MnO_{2.00}$
Cry3	Nitrates-citric acid	500 °C	Cryptomelane (PDF 29-1020)	$K_{0.11}Na_{0.05}MnO_{2.01}$
Sp1	Nitrates-citric acid	900 °C	$LiMn_2O_4$ (PDF 35-0782)	–
Sp2	Nitrates-citric acid	850 °C	$LiMn_2O_4$ (PDF 35-0782)	–
Sp3	Nitrates-citric acid	400 °C	$LiMn_2O_4$ (PDF 35-0782)	–
Sp4	Ion-exchange of Sp2	–	Spinel (λ-MnO_2) (PDF 42-1169)	–
Per1	Nitrates-citric acid	900 °C	$CaMnO_3$ (PDF 45-1266)	–
Per2	Via $(Ca,Mn)CO_3$	900 °C	$CaMnO_3$ (PDF 45-1266)	–
Per3	Via $(Ca,Mn)CO_3$	900 °C	$CaMnO_3$ (PDF 45-1266)	–

electron microscopy, and only samples with a relatively narrow particle size distribution below 1 μm were used for electrochemical studies.

Voltammetric measurement

The electrochemical technique of voltammetry of microparticles has been generally reviewed [17, 18]. The device, experimental technique, and data processing used in this study are already described elsewhere [21, 22, 26, 34, 35]. The samples were mechanically deposited on the working electrode (a paraffin-impregnated rod of spectral graphite). The electrochemical experiments were performed in 0.2 M sodium acetate/acetic acid buffer (pH 4.4) in a glass cell with the working electrode, saturated calomel reference (SCE), and Pt-plate counter electrode. All potentials are related to the SCE. The measurements were performed with potentiostat μAutolab (Eco Chemie Utrecht, Netherlands). The following measuring techniques were used: normal cyclic voltammetry (scan rate 1 mV/s), normal chronoamperometry, and chronoamperometry with three potential pulses (10 mV amplitude, 20 s duration, applied in 39th, 119th, and 289th seconds of the experiment, first samplings 1 s after switching the pulse on and off).

Results and discussion

The synthetic methods used for sample preparation are summarised in Table 1. For the sol-gel synthesis of α-MnO_2, glycerol (trihydroxypropanol) was used instead of fumaric or maleic acid, which were originally used [28–30]. We further proved that citric acid and mannitol can also be used for preparation of the amorphous precursor. The crystallisation of the precursor by final calcination at 450 °C is not significantly dependent on the nature of the organic substance having been used to form the gel precursor.

The nitrates-citric acid method used here for Cry3, spinel, and perovskite oxides closely resembles the Pechini process [37], but without the addition of glycerol or other polyols. Contrarily to the combustion method, the decomposition of nitrates and the fuel is not so exothermic in the nitrates-citric acid method used here. The solution of metal nitrates with citric acid in the smallest volume of water was evaporated, yielding a fragile light ochre foam. The nitrates had already started to decompose during evaporation of the initial solution. The majority of organic residues were burnt off at about 300 °C, and the resulting very fine XRD-amorphous ash was crystallised at the final temperature given in Table 1. To avoid a too exothermic reaction course, it was necessary to add citric acid in the amount of at least 1 mmol citric acid per 1.5 mmol nitrates. At ratios (Na + K)/Mn of about 1:10 to 1:5, relatively well-crystalline α-MnO_2 arose, whereas at higher amounts of Na or K, a colourful mixture of hardly identifiable layered Mn oxides was obtained. $LiMn_2O_4$ was synthesised similarly from corresponding nitrates.

Synthetic products and commercial samples of EMD were characterised by powder XRD and identified according to the database PDF. The formulae of samples were calculated using the total amount of Mn and other metal ions present; the oxygen content was calculated assuming the normal valencies of alkaline metals as +1, alkaline earth metals as +2, and the Mn valence obtained by iodometric titration. The results are summarised in Table 1.

All the Mn oxides studied yield well-reproducible cathodic voltammetric peaks at potentials several tens to several hundreds of millivolts more negative than the open circuit potential under given conditions, i.e., the reductive dissolution proceeds between +600 and +300 mV vs. SCE (see Figs. 1 and 2). The corresponding voltammetric curves are shown in Figs. 1 and 2. Our results can be qualitatively compared with those obtained by deGuzman et al. [16] in KCl solution and in slightly alkaline buffers and by Komorsky-Lovrić et al. [19] in KNO_3 solution. Contrarily to the complex voltammetric curves obtained in neutral and alkaline solutions [14, 15, 19], much simpler voltammetric peaks are well developed in the acetate buffer. In the subsequent scans, there are no significant voltammetric peaks beside an insignificant signal of the Mn^{2+} residues from the vicinity of the working electrode. A totally irreversible process is hence responsible for the voltammetric peaks between 600 and 300 mV vs. SCE in acetate buffer according to the almost identical shapes of the backward and forward current/potential curves obtained by square-wave voltammetry, similarly as was reported for irreversible reactions of solids [19]. The standard redox potential of reaction 1 (below) calculated from thermodynamic data for β-MnO_2 is 0.52 V vs.

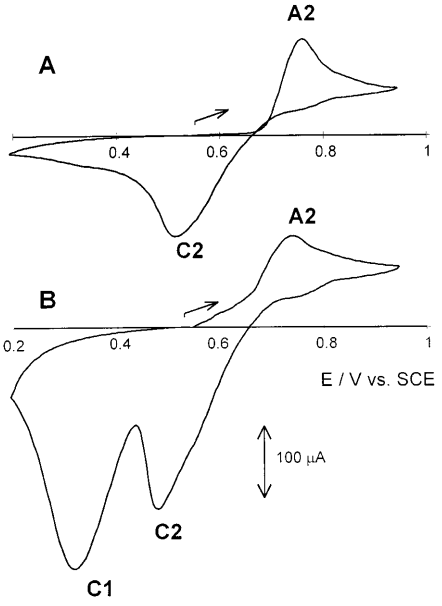

Fig. 1 Cyclic voltammetry curves of a clean working electrode in 5 mM $Mn(MeCO_2)_2$ (**A**), and a working electrode with α-MnO_2 (Cry3) in 5 mM $Mn(MeCo_2)_2$ (**B**), both in 0.2 acetate buffer, pH 4.4, scan rate 5 mV/s, first scan from OCP in anodic direction. Peak notation: *C1* reductive dissolution of α-MnO_2, *A2* oxidative precipitation of MnO_2 from Mn^{2+} according to Eq. 2, *C2* reductive dissolution of MnO_2 formed in the peak *A2*

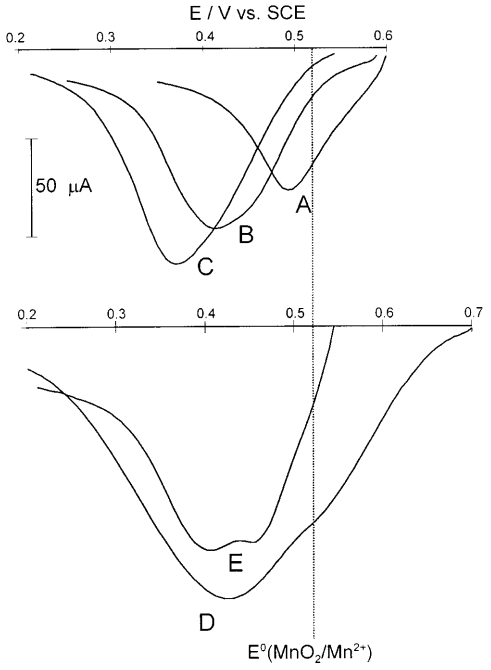

Fig. 2 Voltammetric peaks of Mn oxides studied. *A* Bir2, *B* Cry2, *C* EMD1, *D* Per1, *E* Sp2. The *line* represents the standard potential of the reaction $\beta \rightleftharpoons MnO_2 + 2e^- + 4H_3O^+ \rightleftharpoons Mn^{2+} + 6H_2O$ at pH 4.4 [38]

SCE [38]. Additionally, a solid intermediate, Mn_2O_3, is thermodynamically stable only at pH > 5 [38]. We can hence conclude that in acetate buffer at pH 4.4 and at $E < 0.5$ V/SCE the cathodic peaks which we obtained correspond to a total reductive dissolution of Mn oxides (see Eq. 1).

Overall reductive dissolution of MnO_2 in the presence of protons can be generally expressed by Eq. 1:

$$MnO_2(s) + 2e^- + 4H_3O^+ \xrightarrow{\text{cathodic scan}} 2Mn^{2+}(aq) + 6H_2O \quad (1)$$

Such complete reaction must be practically irreversible because the original MnO_2 structure is completely destroyed after deep discharge [39, 40]. Hence, Mn(IV) oxide in situ formed by reverse oxidation of $Mn^{2+}(aq)$ must be of a different structure than the original Mn oxide. The formation of amorphous δ-MnO_2 by anodic polarisation of $Mn(OH)_2$ was assumed [6, 13]:

$$Mn^{2+}(aq) + 6H_2O \xrightarrow{\text{anodic scan}} \delta\text{-}2MnO_2(s) + 2e^- + 4H_3O^+ \quad (2)$$

Practical irreversibility of the total MnO_2 reduction is the reason for the limited efficiency of the secondary batteries based on Mn oxides at higher pH values [7, 39]. Clear evidence of the irreversibility of reactions 1 and 2 in our experiments is about 0.4 V separation of the peaks of the Mn(IV)(s)/Mn^{2+}(aq) redox pair (see curve A in Fig. 1). The difference between original and secondary Mn(IV) oxide species is also shown in Fig. 1, curve B, where two separated peaks are visible on a cathodic branch of a cyclic voltammetric curve of α-MnO_2 after anodic polarisation of the working electrode in $Mn(MeCO_2)_2$ solution: the more negative C1 (mechanically immobilised α-MnO_2) and the more positive C2 (in situ formed δ-MnO_2). The only influence of another Mn oxide having been present on the working electrode before oxidative precipitation of δ-MnO_2 is the absence of the induction period in oxidative precipitation of Mn^{2+}, that is otherwise observed on a clean graphite electrode and probably caused by slow nucleation of δ-MnO_2.

Contrary to alkaline electrolytes [4, 6, 12, 13, 40], the supporting electrolyte chosen here does not permit the formation of soluble Mn(III) intermediates, and so we can suppose that reaction 1 proceeds in the solid phase until soluble Mn^{2+} hydrated ions are formed. However, the dissolution reaction could involve two subsequent charge-transfer steps, and some solid intermediates can possibly be involved in the reaction chain. We can hence hypothetically suppose the (at least temporary) presence of some [$Mn^{III}OOH$] intermediate, similar to that assumed in the course of the reduction of Mn oxides in alkaline medium:

$$MnO_2(s) + e^- + H_3O^+ \rightleftharpoons [Mn^{III}OOH](s) + H_2O \quad (3)$$

The so-formed [$Mn^{III}OOH$] is further reduced:

$$[MnOOH](s) + e^- + 3H_3O^+ \longrightarrow Mn(II)(s) + 5H_2O \quad (4)$$

or it could disproportionate:

$$2[MnOOH](s) + 2H_3O^+ \rightleftharpoons Mn^{2+}(aq) + MnO_2(s) + 4H_2O \quad (5)$$

Spontaneous disproportionation can be expected in the chosen slightly acidic solution for thermodynamic reasons. Similarly, Mn_2O_3 disproportionates at pH < 5 [38]. In general, the potential range of stability of Mn(III) at pH 4.4 is at best so narrow that reactions 3 and 4 might proceed simultaneously. The dissolution is finished by a final step:

$$Mn^{II}(s) \xrightarrow{H_3O^+} Mn^{2+}(aq) \quad (6)$$

Because the reductive dissolution of practically all studied Mn oxides yields voltammetric peaks with single and well-defined maxima, we suppose that [$Mn^{III}OOH$] can be either formed only in a thin surface layer on the dissolving Mn oxides, or that [$Mn^{III}OOH$] is not generated at all under the given conditions. As is known, solid Mn(III) intermediates are reasonably stable at higher pH and hence more complex voltammetric curves are always observed during the reductive decay of Mn(IV) oxides in alkaline solution, where the individual peaks of the Mn(IV)-Mn(III) and Mn(III)-Mn(II) steps are observed [6, 10, 12–15, 38]. To recognise which of the Eqs. 1 and 3–6 is the rate-determining step for the Mn

oxides studied, the results of voltammetric and chronoamperometric measurements should be discussed in more detail.

The voltammetric peak potentials of individual Mn oxides (Fig. 2) cannot be directly used to evaluate a phase specificity of the dissolution reaction. The potential window, where the peaks occur, is relatively narrow (about 200 mV), considerably less than in the case of reductive dissolution of Fe(III) oxides [21] and oxidative dissolution of Cr(IIII,IV) oxides [26]. Because also particle size and reaction course can affect the actual peak potential of the microparticulate reactant [21, 22, 34, 41, 42], another characteristic must be used for the comparison of the relative reactivity of the samples studied.

To simplify the complex problem of the interpretation of the voltammetric peak potentials of powdered reactant, the determination of a kinetic characteristic, a_L, that is formally equal to the reciprocal Tafel slope, was proposed by Grygar et al. [26, 34, 35]. The value of a_L is not explicitly dependent on the geometrical properties of individual solid reactants, but it reflects more directly the nature of the rate-determining step on the reaction interface. a_L represents the relative sensitivity of the reaction rate to the electrochemical potential:

$$a_L = \frac{nF}{RT}\alpha_L = \frac{\partial \ln(k)}{\partial E} \tag{7}$$

where n is the number of electrons exchanged in the rate-determining step, α_L is the formal charge transfer coefficient of the particular sample at a given potential, and k is the rate coefficient. Unfortunately, electrochemical dissolution of metal oxides frequently represents a typical example of mixed reaction kinetics without a single rate-determining step, i.e., with several processes of a different nature that determine the overall reaction rate. As a result, a_L is a function of the electrochemical potential.

The separation of the pure influence of intensive variables, which is assumed in Eq. 7, is justified only for those heterogeneous reactions which proceed exclusively on a reacting interface of constant composition, i.e., when the overall reaction rate is not affected by continuously changing diffusion profiles of the reactants [43]. Under this condition, the pure contribution of the electrochemical potential to the reactivity can be theoretically separated even in the case of a particulate reactant [34]. However, owing to a finite size of the powdered samples in the voltammetry of microparticles, 'steady-state currents', cannot be directly measured, as is common with semi-infinite solid electrodes such as pellets or thick films. The double potential step technique, which is used to eliminate the hardly predictable actual influence of the finite size of a solid reactant on the reaction kinetics, is not applicable to totally irreversible reactions.

The measuring technique suitable for the estimation of a_L of irreversible reactions of particulate reactants is potential pulse chronoamperometry (PPC) [26, 35]. PPC is based on the examination of the current response to potential pulses ΔE applied from the base potential E_B (see Experimental for more details). Taking into account a finite size of the potential pulse and the proportionality between the actual current and the rate coefficient of an irreversible reaction [34], Eq. 7 changes to:

$$a_L \cong \frac{\ln(I_{B+\Delta}) - \ln(I_B)}{\Delta E} \tag{8}$$

where $I_{B+\Delta}$ is the current during the potential step with the height of Δ_E, and I_B is the extrapolated value of the current expected for the moment of the potential pulse but at E_B, as is shown in Fig. 3. A typical current response to the potential pulses and the method of estimation of a_L are shown in Fig. 3 for a sample of α-MnO_2. Currents I_B and $I_{B+\Delta}$ are represented by two curves that reflect the change of the reaction rates with continuous consumption of the reactant. In agreement with the kinetics of a general reaction order (Eq. 9), which is quite common for chemical and electrochemical dissolution of powdered reactants [21, 22, 34], these curves are approximately linear and parallel in the variables chosen in Fig. 3 (middle and right plots). In all

Fig. 3 The current response to the potential pulses applied during the dissolution of α-MnO_2 at the base potential of 0.49 V/SCE, shown as obtained by chronoamperometry (*left*) and after transformation into a kinetic function $\ln(I/Q_0)$ vs. $\ln(Q/Q_0)$ [34] (*middle*). In the *right* plot, the detail of the second pulse and the extrapolation of the current after the pulse application are shown. The current response corresponds to dissolution via a surface electrochemical reaction

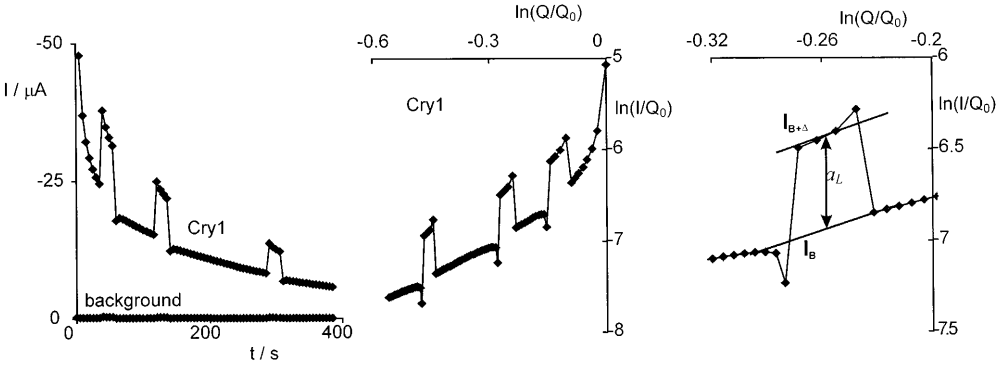

cases described here, the value a_L was not significantly dependent on the position of the pulse. Hence this permits us to use Eq. 7 directly to estimate a_L by comparison of the logarithms of the rate constant, which can be obtained by processing the chronoamperometric curves. For all the studied phases except birnessite, the kinetics of the apparent reaction order was used to extrapolate the initial reaction rate, for which:

$$\frac{I}{Q_0} = k\left(\frac{Q}{Q_0}\right)^{\gamma} \tag{9}$$

where Q and Q_0 are the actual and total remaining charges of electrochemical reaction, I is the actual current, k is the rate coefficient, and γ is the apparent reaction order. Q/Q_0 represents the fraction of the remaining solid reactant and I/Q_0 is the actual reaction rate in s^{-1}. The kinetic Eq. 9 was successfully used for fitting the chronoamperometric curves at least for reaction conversions from 10% to 70% (see Fig. 4). $\ln(k)$ versus E plots were fitted by quadratic curves using the least squares method. a_L values are equal to the slopes of these parabolas. So the obtained values were comparable to the values obtained by PPC using Eq. 8.

As was already shown for the electrochemical dissolution of Cr oxides [26] and Fe oxides [34], a_L depends on the electrochemical potential in a manner that is typical of the nature of the rate-determining step. These dependences for reductive dissolution of Mn oxides at potentials where the major part of voltammetric dissolution peaks occur are shown in Fig. 5. In this potentials range a_L values obtained according to Eq. 8 on the one hand and Eqs. 7 and 9 on the other hand were the same. The similarity of the curves a_L vs. E means that the reaction mechanism is the same for all phases studied except for perovskite. For all samples except for perovskite, the values of a_L are typical for a one-electron rate-determining step continuously changing to a mass transport limiting step (e.g., according to Eq. 6) at lower potentials, where a_L tends to decrease to

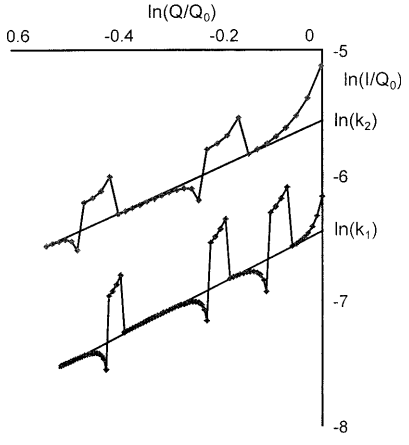

Fig. 4 The shape of the current response in PPC of Sp2; base potentials $E_1 = 0.51$ V/SCE, $E_2 = 0.47$ V/SCE. Extrapolation of the initial rate is shown

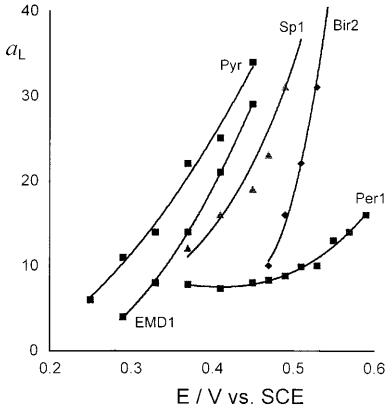

Fig. 5 a_L versus E at potentials of a massive dissolution by a fast surface reaction (around the maxima of the voltammetric peaks)

almost zero (more detailed explanation is given elsewhere [26, 34]).

Two models can explain a one-electron rate-determining step: charge transfer-controlled reaction 3 followed by the non-electrochemical disproportionation reaction 5, or a fast, steady-state equilibrium formation of Mn(III) followed by the rate-determining charge-transfer reaction 4. To elucidate the reaction mechanism, we focused also on the kinetics of the reaction at more positive potentials than given in Fig. 5, i.e., before the substantial part of voltammetric peaks. Here, the values of a_L were as high as 40–55, typical for two-electron or two coupled one-electron reactions controlling the overall reaction rate. Additionally, the current responses changed from roughly squared in $\ln(I/Q_0)$ vs. $\ln(Q/Q_0)$ coordinates as is shown in Fig. 6 (upper curve) to the peak-shaped, distorted trapeziums as in Fig. 6 (lower curve). The latter shape can be expected for solid-state diffusion-controlled reactions. At even more positive potential, the chronoamperometric curves deviate from the curves expected according to kinetic Eq. 8, and a_L values obtained by PPC were much larger than those obtained by comparing $\ln(k)$ to E using Eqs. 7 and 9. The dependence of a_L on E in a wider potential range

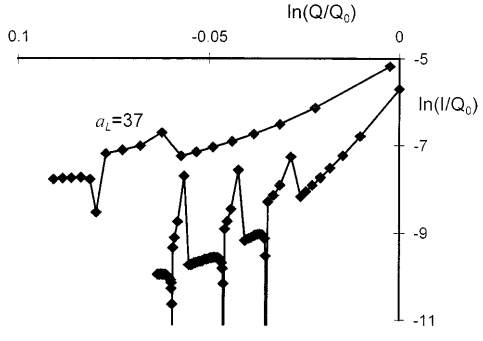

Fig. 6 The difference in PPC curves for EMD1 obtained at 0.55 and 0.51 V/SCE (*lower* and *upper* curves, respectively): a change from dissolution via a surface electrochemical reaction ($E_B = 0.51$ V) to a diffusion-controlled reaction ($E_B = 0.55$ V)

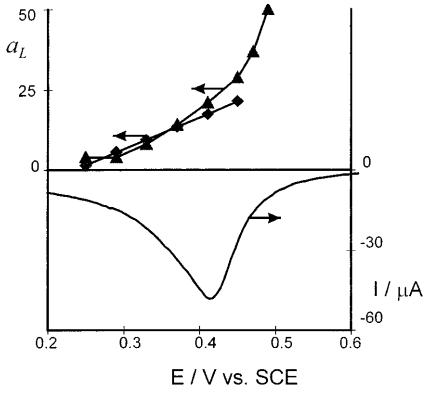

Fig. 7 The dependence of a_L on E in a wider potential range and voltammetric peak for EMD1. The values of a_L were obtained by processing chronoamperometric curves using Eqs. 9 and 7 (◆) and by potential pulse chronoamperometry using Eq. 8 (▲)

and its comparison to the position of the voltammetric peak are shown in Fig. 7.

These facts permit us to suppose that the formation of a Mn(III) intermediate in the solid phase (Eq. 3) precedes the massive dissolution of the oxides according to Eq. 4. The accumulation of Mn(III) intermediates on the Mn oxide surface, which is not sufficiently quickly further reduced to the soluble products, is hence responsible for the growing influence of the solid-state diffusion step at more positive potentials. Contrarly to all other oxides studied, the samples of perovskite oxides exhibit the lowest values of a_L even at potentials as high as 0.6 V/SCE, which probably means a very different reaction mechanism. The low a_L value also explains why the voltammetric peak of $CaMnO_3$ reductive dissolution is so wide (Fig. 2).

The importance of the individual metal manganates(III,IV) structure for the reactivity toward reductive dissolution can be demonstrated by the fact that, contrary to $CaMn^{IV}O_3$, neither $LaMn^{III}O_3$ nor $SrMn^{IV}O_3$ yield well-defined cathodic voltammetric peaks, i.e., the latter phases are not electrochemically reductively dissolved under the chosen conditions. The two latter electroinactive phases have a hexagonally packed anionic sublattice and so a very distorted perovskite structure. Conversely, oxidised $LaMnO_{3+\delta}$, obtained by heating $LaMnO_3$ in air, can be electrochemically reduced.

Conclusions

Complete dissolution of Mn oxides in a slightly acidic environment can be achieved under conditions of voltammetry of immobilised microparticles. The kinetics of the dissolution is the same for α-MnO_2, β-MnO_2, δ-MnO_2, EMD, λ-MnO_2, $LiMn_2O_4$, and birnessite. The dissolution reaction is initiated by the reduction of Mn(IV) to Mn(III) accompanied by proton insertion into the surface of the oxide according to Eq. 3, and the massive dissolution at more negative potentials is limited by the further reduction of Mn(III) to Mn(II) according to Eq. 4. At very negative potentials, the dissolution rate is limited by subsequent dissolution reactions, which yield the final reaction product, the hydrated Mn^{2+} ion. The relative reactivity of the Mn oxide phases toward the electrochemical reductive dissolution in the given medium decreases in the order:

$$\delta\text{-}MnO_2(\text{amorphous}) > \text{birnessite(layered structure)} > \alpha\text{-}MnO_2, \text{EMD}, LiMn_2O_4(\text{3-D structures}) > \beta\text{-}MnO_2(\text{3-D structure})$$

The voltammetry of microparticles could hence be proposed as a method suitable for evaluation of the presence of phase impurities in synthetic samples, if their reactivity is sufficiently different. Because electrochemical and chemical surface reactions control the rate of electrochemical dissolution, voltammetry should also be sensitive to the homogeneity of the size distribution of the samples.

The reductive dissolution of $CaMnO_3$ exhibits a different mechanism for the reductive dissolution, and so it is not possible to directly compare its electrochemical dissolution reactivity to that of other Mn oxides.

References

1. McKenzie RM (1979) Manganese oxides and hydroxides. Minerals in soil environment. Soil Science Society of America, Madison, WI, USA, pp 439–465
2. Albering JH (1999) Structural chemistry of manganese dioxide and related compounds. In: Besenhard JO (ed) Handbook of battery materials. VCH, Weinheim, pp 85–112
3. Feng Q, Kanoh H, Ooi K (1999) J Mater Chem 9: 319
4. Rüetschi P (1975) The electrochemistry of MnO_2. In: Kozawa A, Brodd RJ (eds) Manganese dioxide symposium, vol 1. Union Carbide Corporation, Cleveland, OH, USA, pp 12–46
5. Bell GS, Huber R (1964) J Electrochem Soc 111: 1
6. McBreen J (1975) Electrochim Acta 20: 221
7. Kordesch K, Gsellmann J, Peri M, Tomantschger K, Chemelli R (1981) Electrochim Acta 26: 1495
8. Yao YF, Gupta N, Wroblowa HS (1987) J Electroanal Chem 233: 107
9. Morimoto H, Esaka T, Takai S (1997) Mater Res Bull 32: 1359
10. Li, W, McKinnon WR, Dahn JR (1994) J Electrochem Soc 141: 2310
11. Kanoh H, Feng Q, Miyai Y, Ooi K (1995) J Electrochem Soc 142: 702
12. Donne SW, Lawrance GA, Swinkels DAJ (1997) J Electrochem Soc 144: 2954
13. Bodé M, Cachet C, Pereir J-P (1997) J Electrochem Soc 144: 792
14. Fiedler DA, Besenhard JO, Fooken MH (1997) J Power Sources 69: 157
15. Fiedler DA (1998) J Solid State Electrochem 2: 315
16. deGuzman RN, Shen Y-F, Shaw BR, Suib SL, O'Young C-L (1993) Chem Mater 5: 1395
17. Scholz F, Meyer B (1994) Chem Soc Rev 23: 341
18. Scholz F, Meyer B (1998) Voltammetry of solid microparticles immobilized on electrode surfaces. In: Bard AJ, Rubinstein I (eds) Electroanalytical chemistry, vol 20. Dekker, New York, p 1
19. Komorsky-Lovrić Š, Bartoll J, Stösser R, Scholz F (1997) Croat Chim Acta 70: 563

20. Fiedler DA, Albering JH, Besenhard JO (1998) J Solid State Electrochem 2: 413
21. Grygar T (1996) Collect Czech Chem Commun 61: 93
22. Grygar T (1996) J Electroanal Chem 405: 117
23. Scholz F, Nitschke L, Henrion G (1989) Naturwissenschaften 76: 71
24. Scholz F, Rabi F, Mueller W-D (1992) Electroanalysis 4: 339
25. Zhang S, Meyer B, Moh G, Scholz F (1995) Electroanalysis 7: 319
26. Grygar T, Bezdička P (1998) J Solid State Electrochem 3: 31
27. Parida KM, Kanungo SB, Sant BR (1981) Electrochim Acta 26: 435
28. Bach S, Henry M, Baffier N, Livage J (1990) J Solid State Chem 88: 325
29. Duan N, Suib SL, O'Young C-L (1995) J Chem Soc Chem Commun 1367
30. Ching S, Roark JL, Duan N, Suib SL (1997) Chem Mater 9: 750
31. Feng Q, Yanagisawa K, Yamasaki N (1996) J Chem Soc Chem Commun 1607
32. Ching S, Petrovay DJ, Jorgensen ML, Suib SL (1997) Inorg Chem 36: 883
33. Hunter JC (1981) J Solid State Chem 39: 142
34. Grygar T (1998) J Solid State Electrochem 2: 127
35. Albering JH, Grygar T (1999) J Solid State Electrochem 3: 117
36. Drits VA, Silvester E, Gorshkov AI, Manceau A (1997) Am Miner 82: 946
37. Pecchini MP (1967) US Patent 3 330 697 (x)
38. Liang CC (1973) Manganese. In: Bard AJ (ed) Elencyclopedia of electrochemistry of the Elements. Dekker, New York, p 349–403
39. Mondoloni C, Laborde M, Rioux J, Andoni E, Lévy-Clément C (1992) J Electrochem Soc 139: 954
40. Donne SW, Lawrance GA, Swinkels DAJ (1997) J Electrochem Soc 144: 2961
41. Brainina KZ, Vydrevich MB (1981) J Electroanal Chem 121: 1
42. Mouhandess MT, Chassagneux F, Vittori O, Accary A, Reeves RM (1984) J Electroanal Chem 181: 93
43. Soustelle M, Pijolat M (1997) Solid State Ionics 95: 33